Memoirs of the School of Engineering, Okayama University, Vol. 18, No. 1, January 1984

Finite Element Analysis of Transformer Cores

Takayoshi NAKATA* and Norio TAKAHASHI*

(Received December 28, 1983)

SYNOPSIS

The quantitative analysis of localized flux distributions in transformer cores has become easy through the progress of numerical field calculations. In this paper, the effects of core constructions, joint configurations, magnetizing characteristics of materials on the flux distributions are examined using newly developed techniques such as a gap element, an approximate method for solving three-dimensional magnetic fields, the time periodicity finite element method, an efficient technique for treating hysteresis characteristics and so on. A method for the optimum design of transformer cores is also discussed.

Main results obtained can be summarized as follows:

(a) The building factor of the core made of highly-oriented silicon steel is larger than that of the conventional core.

(b) The iron losses at joints are much affected by overlap lengths, number of laminations per stagger layer and a small irregularity of the arrangement of sheets.

(c) It is clarified that examinations of the optimum construction of core and the most desirable magnetic characteristics of core material are possible using the finite element method.

* Department of Electrical Engineering

1. INTRODUCTION

It is important to understand in detail the behaviour of localized fluxes in transformer cores in order to develop smaller cores with higher efficiency. If we have enough information about the relationship between the magnetic characteristics of core material such as hysteresis, anisotropy and the flux distribution in the core, not only smaller cores with higher efficiency but also new materials which would have the most suitable characteristics as transformer cores would be developed.

The quantitative analysis of localized flux distributions in cores has become easy through the progress of numerical field calculations such as the finite element method. Therefore, the relationship between the magnetic characteristics of core materials and those of transformer cores can be examined analytically. The experimental investigation of these relationships uses much money, time and labor. It has also the disadvantage that the effect of only one factor to be examined cannot be solely investigated due to the spatial inequality of the actual material, the accuracy of dimensions of the model and so on.

In this paper, recent developments in the calculation of flux distributions by using the finite element method are reported with many examples. Firstly, the factors which increase the iron losses of transformer cores are discussed. Secondly, the effects of core construction and magnetizing characteristics of materials on the flux distributions are examined. Thirdly, a method for the optimum design of transformer cores using the finite element method is discussed. Lastly, the present status of estimation techniques of iron losses is explained.

2. FACTORS AFFECTING THE BUILDING FACTOR

The factors which increase the iron losses of laminated cores are as follows:

(1) Distortion of flux waveform due to magnetic saturation,
This is caused by,
(a) nonuniform flux distribution,
(b) difference in path lengths among magnetic circuits,
(c) circulating flux.

(2) Rotating flux,
This is caused by three-phase magnetomotive forces.
(3) Flux directed out of the rolling direction,
(4) Transverse flux at joint,
(5) Interlaminar short circuit,
(6) Deterioration of magnetic characteristics due to the mechanical stress.

In this paper, only factors (1) to (4) are investigated.

The above-mentioned factors are affected by the following items:
(1) Factors which can be controlled by the steel manufacturers,
(a) anisotropy of the magnetizing characteristics,
(b) shape of the hysteresis curve.
(2) Factors which can be controlled by transformer manufacturers,
(a) core structure,
---- shell-type,core-type and so on
(b) core shape,
---- high window, low window and so on
(c) joint configuration.

Other factors affecting the increase of iron losses which can be controlled by steel manufacturers are,
(a) shape of iron loss curve,
(b) anisotropy of iron loss characteristic,
(c) ratio of hysteresis loss and eddy current loss.

If a new material which has magnetic characteristics that the percentage of eddy current loss to the total iron loss is lower and the anisotropy of iron losses is smaller could be developed, the building factor of cores made from such a new material would be reduced[1,2]. As the effects of the other factors are so complicated, further examinations are necessary. The effects of core construction, joint configurations, and hysteresis characteristics on the magnetic characteristics of transformer cores are examined numerically in the following sections.

3. EFFECTS OF CORE CONSTRUCTIONS

Localized flux distributions in various types of three-phase transformer cores are investigated. In this Section, only the case

when the overall flux density Bleg in the leg is 1.7T is discussed. For simplicity, the hysteresis of silicon steel is neglected.

3.1 Method of Analysis

If the leakage flux is negligible, the flux distribution in a core can be analyzed as a Laplacian problem. The magnetic vector potential A in the core satisfies the following non-linear Laplace equation[3],

$$\frac{\partial}{\partial x}\left(\nu_y \frac{\partial A}{\partial x}\right)+\frac{\partial}{\partial y}\left(\nu_x \frac{\partial A}{\partial y}\right)=0 \qquad \text{----------(1)}$$

where ν_x and ν_y denote the x- and y- components of reluctivity respectively.

The non-linear solution of Eq. (1) is obtained by using the finite element method and the Newton-Raphson iteration technique [3]. The spatial flux distribution at each instant and the flux waveform at each point can be calculated from the vector potentials obtained.

3.2 Shell-Type, Three-Limbed Core[4,23]

Figure 1 shows the spatial and time variations of flux

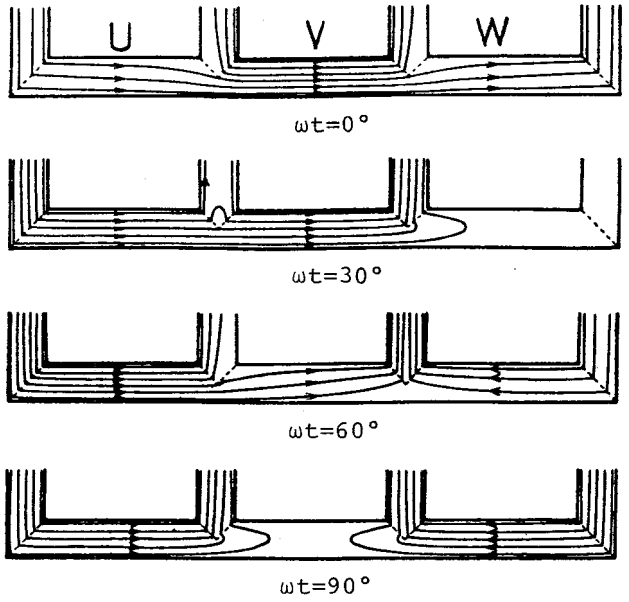

Fig.1 Flux distributions (M-5,0.35mm,Bleg=1.7T).

distributions in a quarter of a shell-type, three-phase, three-limbed core which is made of 0.35mm thick grain-oriented silicon steel (Grade: AISI-78, M-5). The solid lines denote the equi-potential lines. The broken lines represent the joints of silicon steel. Zero time is taken to be the instant when the flux density in the V-limb is at a maximum. The flux changes direction suddenly at joints due to magnetic anisotropy. Moreover, at the instants $\omega t=30°$ and $90°$, a part of the flux circulates at the W-and V-limbs whose fluxes should ideally vanish. At $\omega t=30°$, the same phenomena can be seen in the yoke between the U-and V-limbs, and some circulating fluxes are produced.

Figure 2 shows the flux density waveforms at various points in the core. Flux passing near the windows in the yoke between limbs is much more distorted than in other parts of the core. In general, the waveforms of localized fluxes are distorted due to magnetic non-linearity and the difference in path lengths between magnetic circuits. If there are circulating fluxes in a limb or a yoke, distortion of the flux waveform is increased. The circulating flux causes a phase difference between flux on the inner side and that on the outer side of the limb, or the yoke. Consequently, the maximum flux density on the outer sides becomes greater than that on the inner side. However, when the overall flux density in the limb becomes

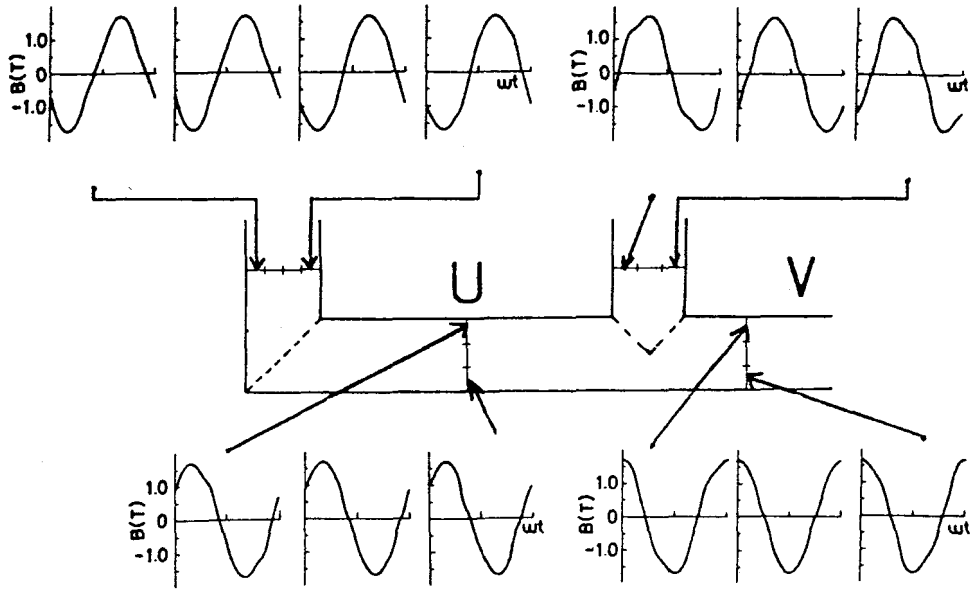

Fig.2 Waveforms of localized flux densities (M-5,0.35mm,Bleg=1.7T).

high, such an increase of the maximum flux density is prevented and harmonic components of the flux are increased due to magnetic saturation.

The flux at each point in the T-joint rotates with time. The spatial variation of the locus of the rotating flux density vector is shown in Fig. 3. The locus contains many higher harmonic components due to magnetic saturation.

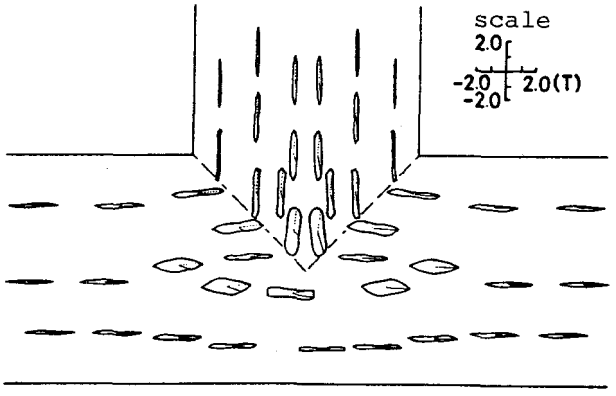

Fig.3 Loci of the flux density vectors in the T-joint (M-5,0.35mm,Bleg=1.7T).

3.3 Core-Type, Three-Limbed Core[5,6,7]

The influence of the qualities of core material and the shape of cores on the flux distributions in core-type, three-phase, three-limbed cores are examined. Figures 4 (a) and (b) show the flux distributions of standard size cores made of 0.35mm thick conventional grain-oriented silicon steel M-5 and of 0.3mm thick highly-oriented silicon steel M-OH respectively. These figures show that the circulating fluxes increase and the inclination of flux becomes remarkable in the high quality core due to the higher anisotropy. Figures 4 (c) and (d) show the flux distributions of cores with lower and higher windows than that of Fig. 4 (a). These three kinds of cores are made of the same material. In all cores, the flux distributions in the limbs are fairly uniform and those in the yokes are complicated. Therefore, the iron loss (W/kg) of a higher window core is smaller than that of a lower window core.

It can be concluded that the building factor of the highly-oriented core is larger than that of the conventional one because of distortion of the flux waveform and the inclination of

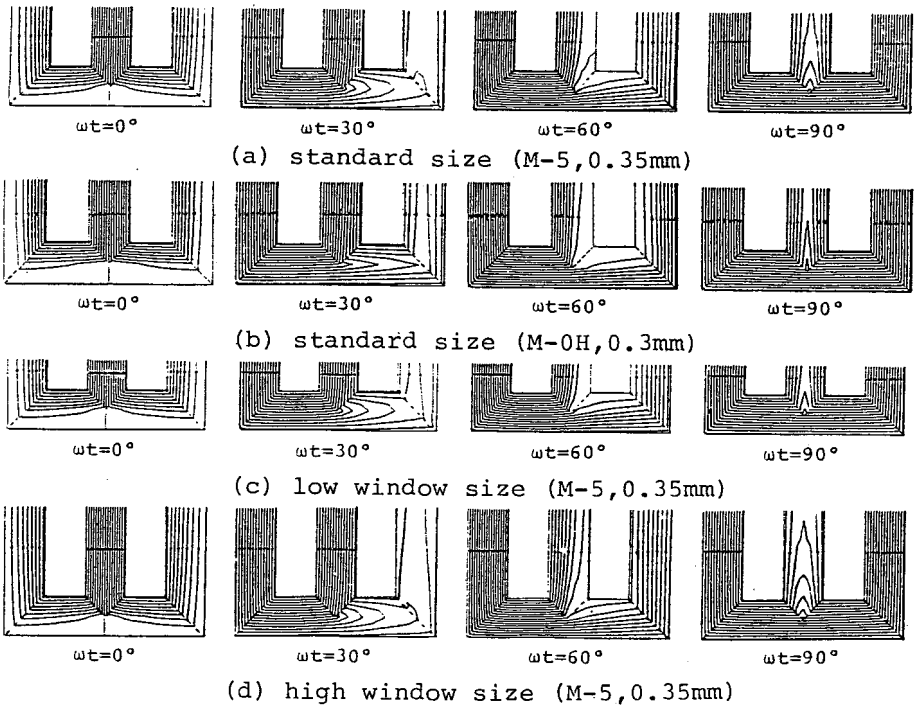

Fig.4 Flux distributions in cores with various qualities and shapes (Bleg=1.7T).

flux. The building factor of the lower window core is also larger than that of the higher one.

The effect of the joint-angle θ in the T-joint shown in Fig. 5 on the magnetic characteristics of cores has been investigated. Figures 6 (a) and (b) show the flux distributions in cores with joint-angles θ=74°and 113° respectively. With the increase of joint-angle, the amount of the circulating flux in the V-limb decreases, and the flux waveforms are improved.

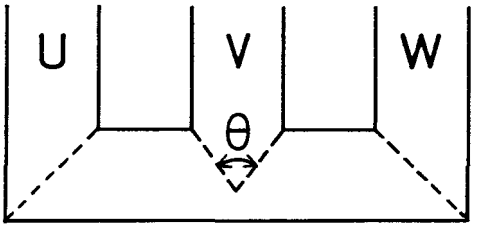

Fig.5 Definition of joint-angle.

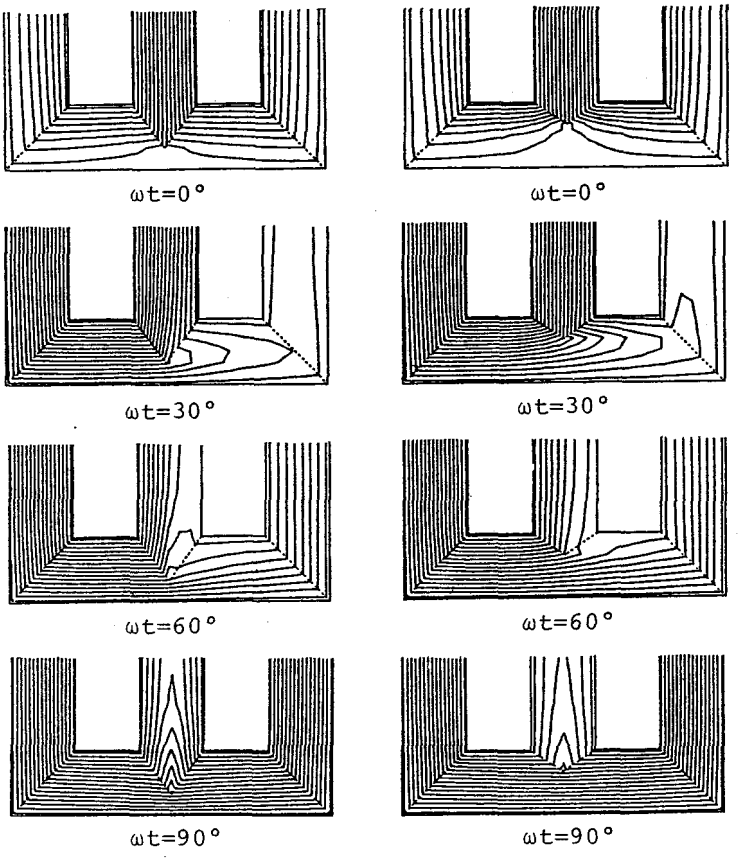

Fig.6 Effects of joint-angles on flux distributions (M-OH,0.3mm,Bleg=1.7T).

Figure 7 shows the flux density vectors in each layer of the T-joint of a so-called scrap-less core. These results are obtained by a new approximate method for solving three-dimensional magnetic fields[8]. The arrows denote the amplitude and the direction of the flux density vector at each point. The average flux distributions of those in both layers in Figs. 7 (a) and (b) are shown in Fig. 8.

The spatial variations of the locus of the rotating flux density vector corresponding to Fig. 7 (a) and Fig. 8 are shown in Figs. 9 and 10 respectively. The spatial distribution of the maximum flux density corresponding to Fig. 7 (a) is shown in Fig. 11. As the directions of the fluxes near the corner of the window in the T-joint are almost the same as the rolling direction, the maximum flux density

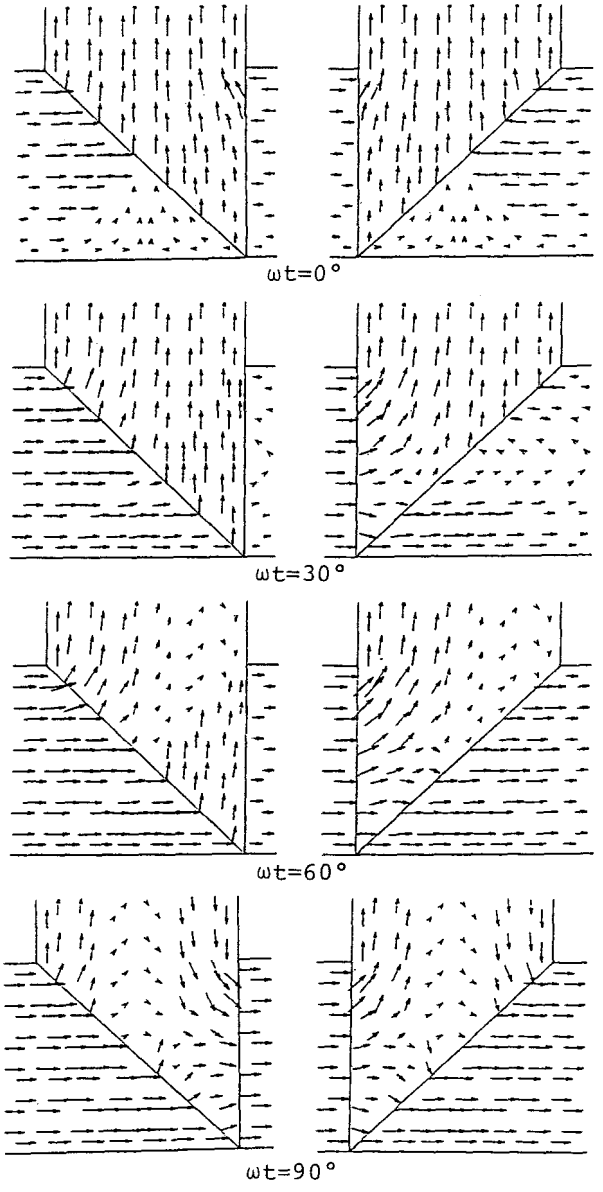

(a) the first layer (b) the second layer

Fig.7 Flux density vectors in each layer (M-5,0.35mm,Bleg=1.7T).

at the corner reaches 2.05 T. The actual iron losses of the core are a function of not the fluxes denoted in Figs. 8 and 10, but those in each layer denoted in Figs. 7, 9, and 11.

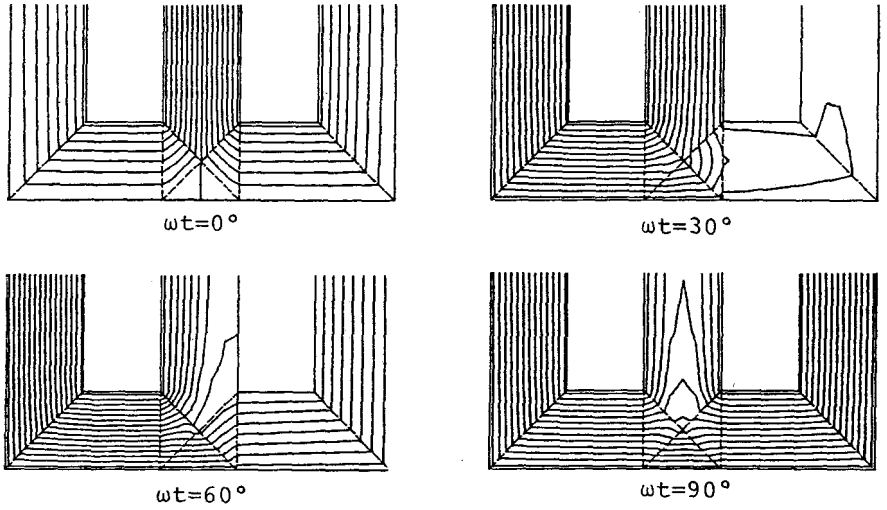

Fig.8 Apparent flux distributions (M-5,0.35mm,Bleg=1.7T).

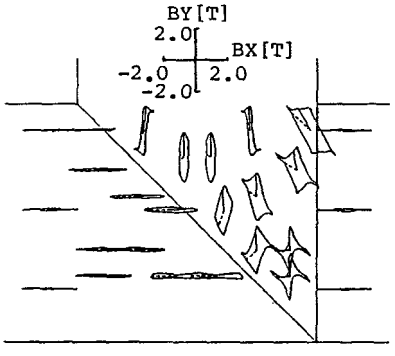

Fig.9 Loci of the flux density vectors in the first layer (M-5,0.35mm,Bleg=1.7T).

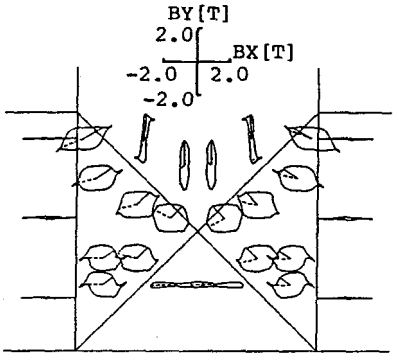

Fig.10 Loci of the apparent flux density vectors (M-5,0.35mm,Bleg=1.7T).

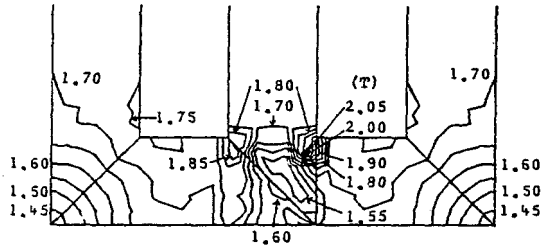

Fig.11 Distribution of the maximum flux density in the first layer (M-5,0.35mm,Bleg=1.7T)

3.4 Five-Limbed Core[4,9,10]

In the analysis of a five-limbed core, the unknown equi-potential boundary condition[9] is introduced. The five-limbed core has large differences in path lengths among its magnetic circuits. Therefore, even if the core is excited by a sinusoidal voltage, waveforms of the overall fluxes in the outer limb and the yoke are distorted. As the outer limb and the yoke have no exciting winding, the amount of the fluxes passing through those parts are very much affected by the gaps at the joints.

Figure 12 shows the effects of air gaps on the flux distributions in five-limbed cores made of 0.35mm thick grain-oriented silicon steel M-5[10]. Gap elements[30] are set at joints. The gap width is assumed to be 0.083% of the width of the inner limb. The cross-sectional area of the yoke and the outer limb is taken to be a half of that of the inner limb. In Fig. 12 (b), the flux in the yoke is increased and that in the outer limb is decreased because of the increase of the reluctance of the outer limb. Flux distributions in

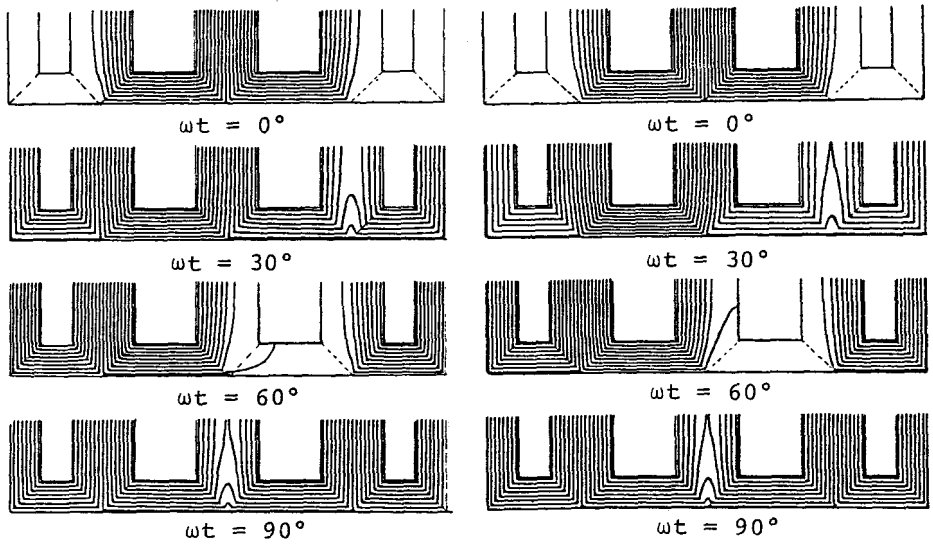

(a) without air gap (b) with air gap

Fig.12 Effects of air gaps on flux distributions (M-5,0.35mm,Bleg=1.7T).

the core with another joint configuration different to that in Fig. 12 are shown in Fig. 13. The amount of circulating flux at $\omega t=90°$ is decreased compared to that in Fig. 12.

Figure 14 shows the waveforms of localized flux densities in the core shown in Fig. 12 (a). The waveforms are distorted and the maximum content K_3 of the third-harmonic component is about 20% on the window side of the inner limb. K_3 is defined by,

$$K_3 = \frac{\text{(3rd harmonic flux density)}}{\text{(fundamental flux density)}} \times 100(\%) \quad \text{---------- (2)}$$

The waveforms in the outer limb contain minor loops. The flux in the T-joint of five-limbed core also rotates with time and this causes the increase of iron losses.

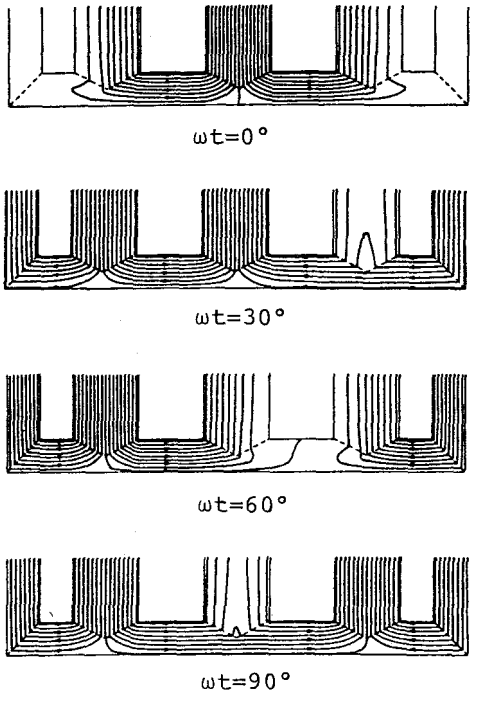

Fig.13 Flux distributions (M-5,0.35mm,Bleg=1.7T).

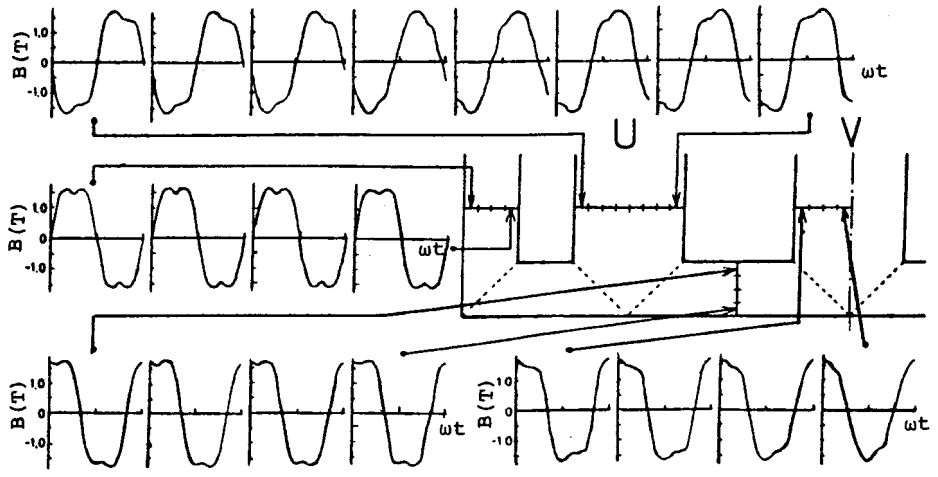

Fig.14 Waveforms of localized flux densities (without air-gap,M-5,0.35mm,Bleg=1.7T).

4. EFFECTS OF JOINTS

The magnetic characteristics of cores with straight overlap joints and step-lap joints have been analyzed using the finite element method taking into account eddy current and magnetic saturation.

4.1 Method of Analysis

The vector potential A satisfies the following equation for the magnetic fields with eddy currents[3].

$$\frac{\partial}{\partial x}\left(\nu_y \frac{\partial A}{\partial x}\right)+\frac{\partial}{\partial y}\left(\nu_x \frac{\partial A}{\partial y}\right)=-J_0-J_e \quad \text{----------(3)}$$

Where,

$$J_e=-\sigma\frac{\partial A}{\partial t}+\frac{\sigma}{S_t}\iint_s \frac{\partial A}{\partial t}\,ds \quad \text{----------(4)}$$

J_0 is the magnetizing current density, J_e is the eddy current density, and σ is the conductivity. S_t is the cross-sectional area of one lamination. ν_x is the reluctivity in the rolling direction. We do not have any information about the reluctivity ν_y in the perpendicular direction. Then, ν_y of the non-oriented silicon steel is chosen to be the same value as that in the rolling direction and ν_y of the grain-oriented silicon steel is chosen to be the same value as that in the transverse direction. In order to reduce the computing time, a

newly developed method which is called the "time periodicity finite element method[11]" is used. The second term of Eq. (4) is calculated by using the symmetry of the joint and the periodicity conditon[12].

4.2 Straight Overlap Joints in Laminated Cores

The flux and eddy current loss distributions around a joint shown in Fig.15 have been investigated[13,14]. The following major variables which affect the magnetic characteristics of cores have been investigated: 1) overlap length L, 2) air gap length G, 3) non-linearity of the magnetic characteristics of silicon steel, 4) number n of laminations per stagger layer. The analyzed section of the lap joint is denoted in Fig.15. Only the region α-O-β-γ-Q-δ-α is analyzed. The number n is equal to 3 in Fig. 15. The core is made of 0.5mm thick non-oriented silicon steel M-47. Figures 16, 17 and 18 illustrate the influences of the number n and the flux density on the flux distributions. Because of symmetry, only parts of the whole flux distribution denoted. The dimensions in both the upper and the lower directions of these figures are expanded 6 times for clarity. The overall flux densities of Figs. (a) and (b) are 0.58 and 1.47T respectively. The overall flux density B is defined by the following equation:

$$B=\frac{\text{(the maximum value of the flux passing through the section far from the joint in one lamination)}}{\text{(the cross-sectional area of the lamination)}} \quad -----(5)$$

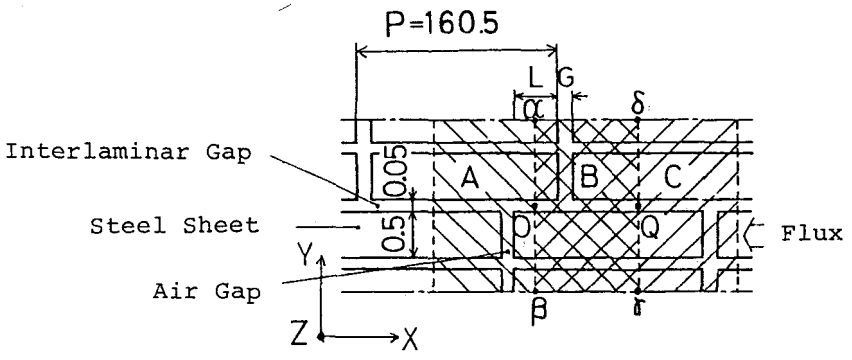

Fig.15 Analyzed model of a laminated core (n=3).

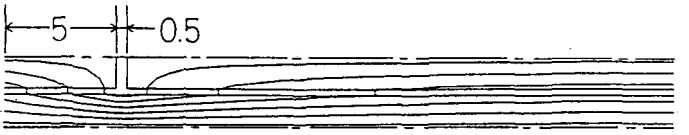

(a) low flux density (B=0.58T)

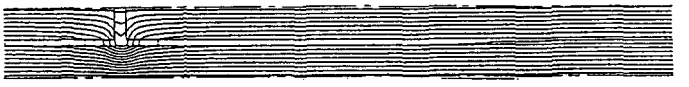

(b) high flux density (B=1.47T)

Fig.16 Flux distributions (M-47,0.5mm,n=1,L=10,G=0.5).

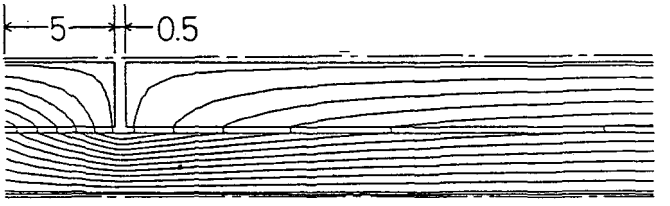

(a) low flux density (B=0.58T)

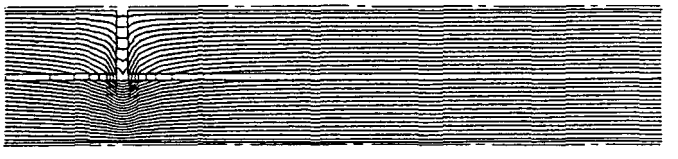

(b) high flux density (B=1.47T)

Fig.17 Flux distributions (M-47,0.5mm,n=2,L=10,G=0.5).

In the case when the notation B is used, the eddy currents are neglected. If eddy currents are taken into account, the flux distribution is influenced by the waveform of the applied voltage. In this Section, when the notation Bm is used instead of B, eddy currents are taken into account.

Figures 16, 17 and 18 show that the transverse flux in the interlaminar gap concentrates near the joints with the increase of the flux density. Figure 19 shows the ratios of the transverse flux to the total one. The suffixes X_i and X_0 denote the distance from the ends of laminations. For example, Φ_{nx0} denotes the transverse flux

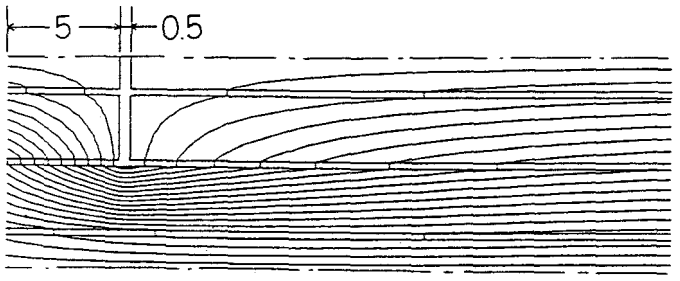

(a) low flux density (B=0.58T)

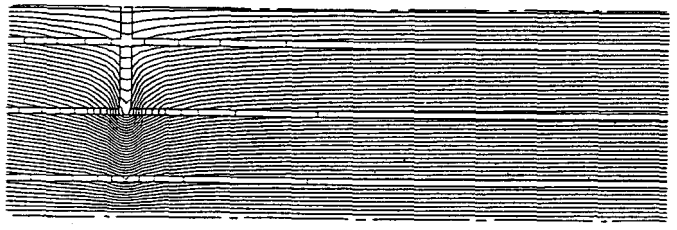

(b) high flux density (B=1.47T)

Fig.18 Flux distributions (M-47,0.5mm,n=3,L=10,G=0.5).

between the edge of the lamination and the point X_0. The suffix n denotes the normal component of the flux. Φ_{n0} and Φ_{ni} are total transverse fluxes on the right and the left sides of the gap. Let us introduce the transverse distance $l\phi$ for clarity. $l\phi$ is defined as the distance X_0 when the ratio Φ_{nx0}/Φ_{n0} becomes (1-1/e) as shown in Fig. 19. As this definition is similar to that of the time constant, the summation of the transverse flux between the points $X_0=0$ and $X_0=5\cdot l\phi$ is more than 99% of the total transverse flux between two laminations. In Fig. 20, the transverse distances are shown together with the ratios of the flux Φ_G passing through the gap to the total flux $(\Phi_G+\Phi_{n0})$ in the laminations per stagger layer. Figure 20 shows that lo decreases rapidly when the flux density becomes higher.

Figure 21 shows that the flux distribution when the magnetic field is increasing is very different from that when the magnetic field is decreasing due to eddy current.

Figure 22 shows the effects of the number n on the distributions of eddy current losses.

The equivalent iron loss length lw which is defined by Eq. (6) is introduced as a convenient measure of the increased loss.

$$l_w = \frac{\text{(iron loss with joint)-(iron loss without joint)}}{\text{(iron loss per unit length without joint)}} \quad ---- \quad (6)$$

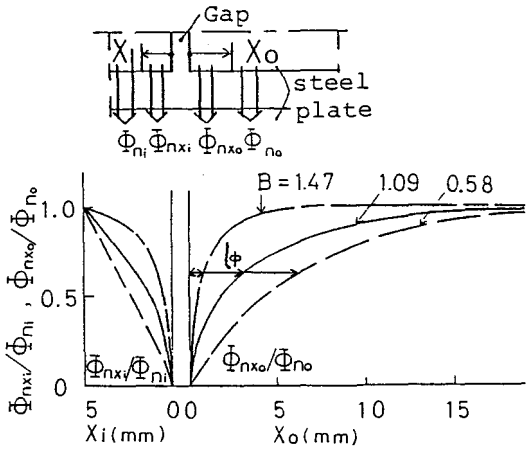

Fig.19 Percentage of the transverse flux (M-47,0.5mm,n=1,L=10, G=0.5).

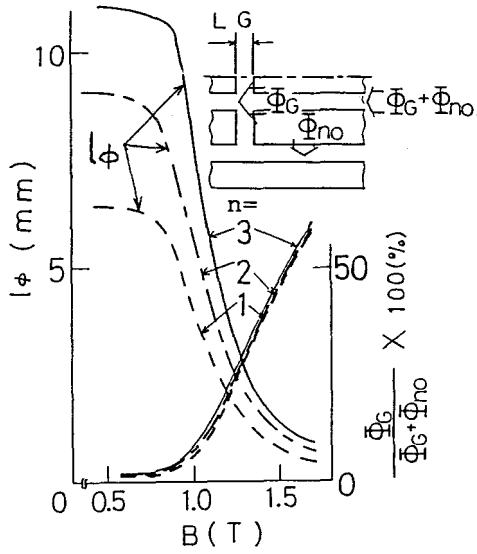

Fig.20 Equivalent transverse length of the flux and the flux passing through gap (M-47,0.5mm,L=10, G=0.5).

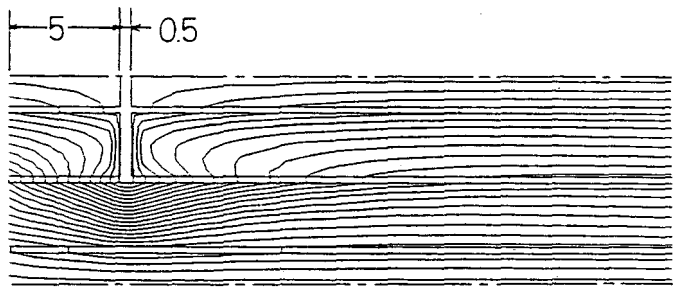

(a) magnetic field is increasing (ωt=45°)

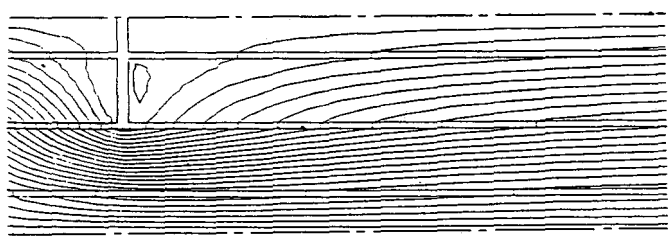

(b) magnetic field is decreasing (ωt=135°)

Fig.21 Effect of eddy current on flux distributions (M-47,0.5mm,n=3,L=10,G=0.5,Bm=1.0T,50Hz)

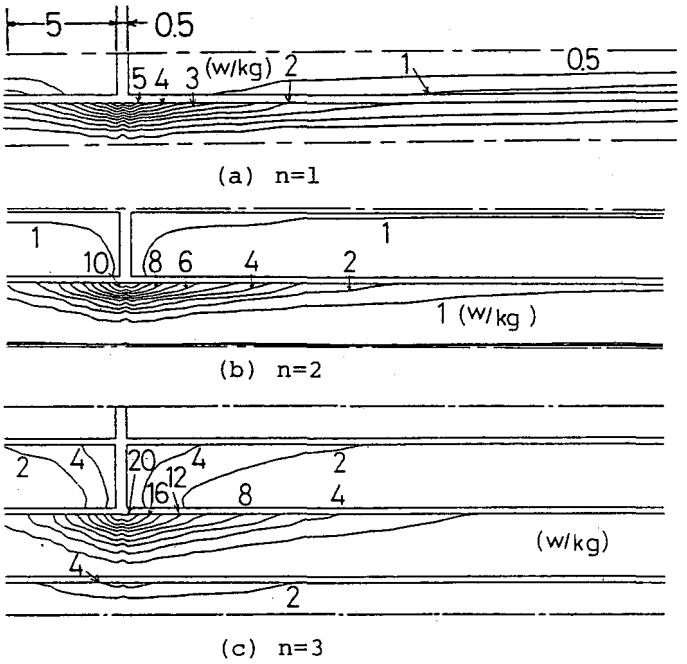

Fig.22 Eddy current loss distributions (M-47,0.5mm,L=10,G=0.5,Bm=1.0T,50Hz).

Figure 23 shows the relationships between the overlap length L and the equivalent eddy current loss length lwe. When the overlap length becomes larger, the equivalent loss length is increased and finally reaches saturation.

Figure 24 shows the effect of the number n of laminations and the

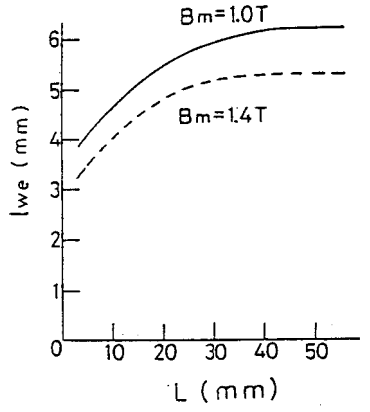

Fig.23 Relationships between lap length and equivalent eddy current loss length (M-47,0.5mm,n=1,G=0.5, 50Hz).

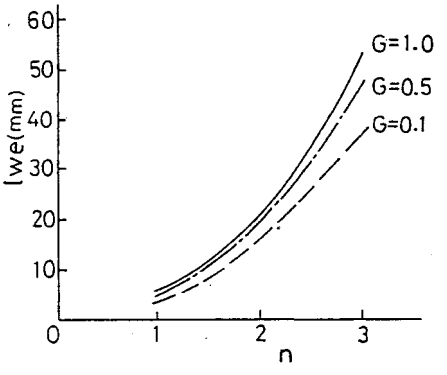

Fig.24 Equivalent eddy current loss length (M-47,0.5mm, L=10,Bm=1.0T,50Hz).

gap length G on the equivalent eddy current loss length lwe. This figure shows that when the number n is increased, the eddy current loss length is also increased very rapidly and it is very much influenced by the gap length. Therefore, when transformer manufacturers construct laminated cores with large n, the air gaps between laminations should be made small with the greatest possible care.

Figure 25 shows the flux distribution near the joint of the core made of 0.3mm thick grain-oriented silicon steel M-3H. In this case, the arrangement of laminations the joint is irregular due to human errors. As the iron losses are considerably increased by small irregularities, special attention should be paid in manufacturing laminated cores with lap joints.

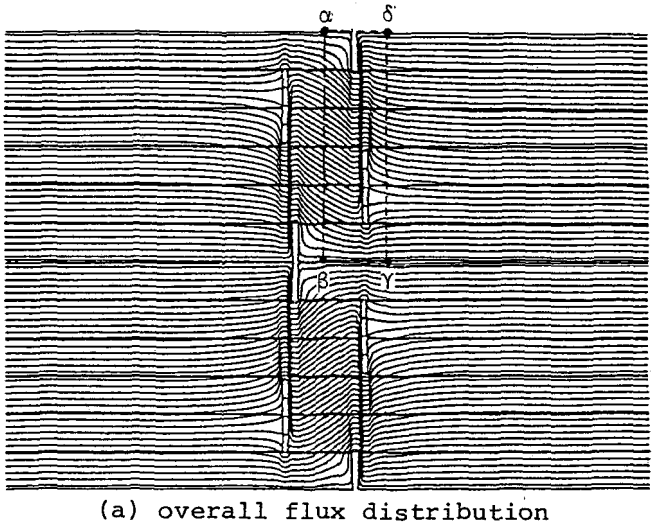

(a) overall flux distribution

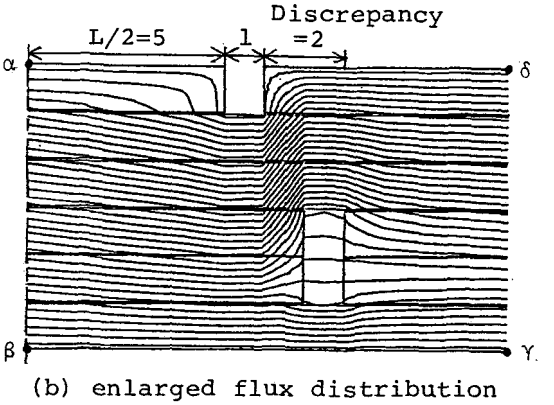

(b) enlarged flux distribution

Fig.25 Flux distributions at the joint with irregular laminations (M-3H,0.3mm,n=2,L=10,G=1,Bm=1.7(T),50Hz).

4.3 Step-Lap Joints in Wound Cores[15,16]

Figure 26 shows a section of the analyzed core. The core is made of 0.3mm thick grain-oriented silicon steel M-3H. S denotes the step-lap length. The space factor of the core is 96%. Then, the interlaminar gap is chosen to be 0.0125mm. Only the hatched part is analyzed because of the symmetry.

Figure 27 shows the influence of the amplitude B of the overall flux density on the flux distributions. In this case, eddy currents are neglected.

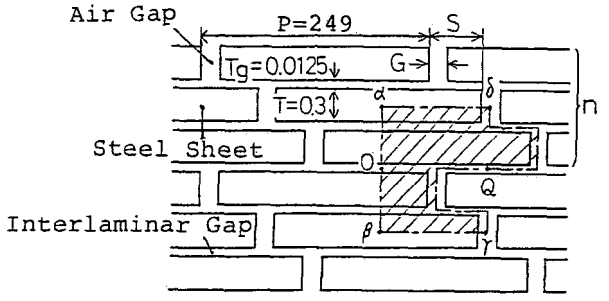

Fig.26 Section of step-lap joints(n=3).

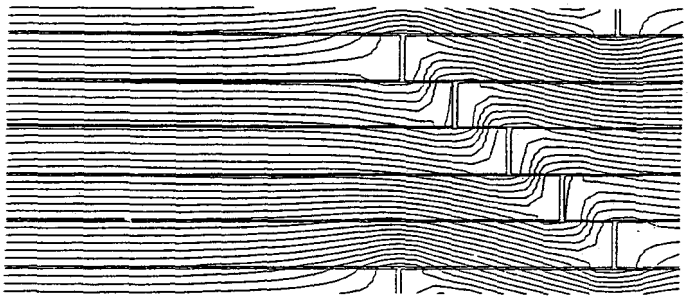

(a) low flux density(B=1.0T)

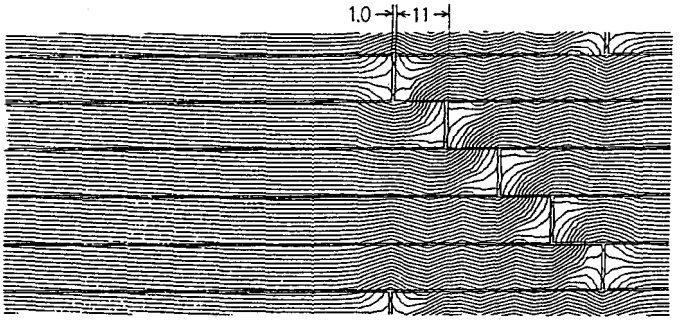

(b) high flux density(B=1.73T)

Fig.27 Flux distributions (M-3H,0.3mm,n=5,S=11,G=1.0).

5. EFFECTS OF HYSTERESIS CHARACTERISTICS

The hysteresis characteristics should be taken into account in order to analyze accurately the flux waveforms, especially those of single-phase transformer cores[17].

Figure 28 shows a quarter of the analyzed single-phase, two-limbed core. The core is made of 0.3mm thick grain-oriented silicon steel M-4. The air gaps at joints are neglected.

Figure 29 shows the flux distributions at Bleg=1.7T[18]. These results are obtained by an efficient technique for treating hysteresis characteristics[31]. Zero time is taken to be the instant when the flux density in the limb is at a maximum. If the hysteresis characteristics are neglected, the flux vanishes at $\omega t=90°$. However, if the hysteresis characteristics are taken into account, circulating fluxes exist at $\omega t=90°$ as shown in Fig. 29 (c). The difference between the flux distributions at $\omega t=75°$ and $105°$ is also caused by the hysteresis effect.

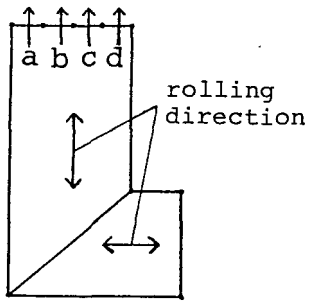

Fig.28 Single-phase, two-limbed core.

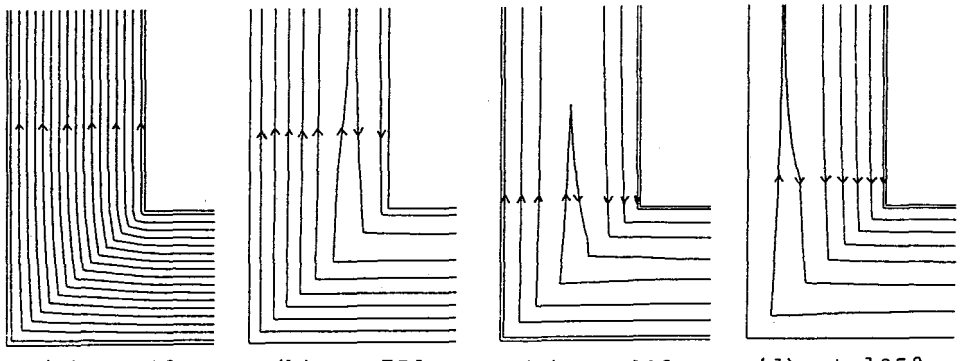

(a) $\omega t=0°$ (b) $\omega t=75°$ (c) $\omega t=90°$ (d) $\omega t=105°$

Fig.29 Flux distributions (M-4,0.3mm,Bleg=1.7T).

Figures 30 and 31 show the waveforms of the localized flux densities at the points a,b,c and d in Fig. 28. The quality of the core in Fig. 30 is M-4 and that in Fig. 31 is M-OH. These figures show that the waveform of each localized flux density becomes non-symmetrical and the phase differences among the waveforms of localized flux densities occur due to the hysteresis effect. As the coercive force of M-OH is smaller than that of M-4, the distortion of waveforms in Fig. 31 is smaller than that in Fig. 30.

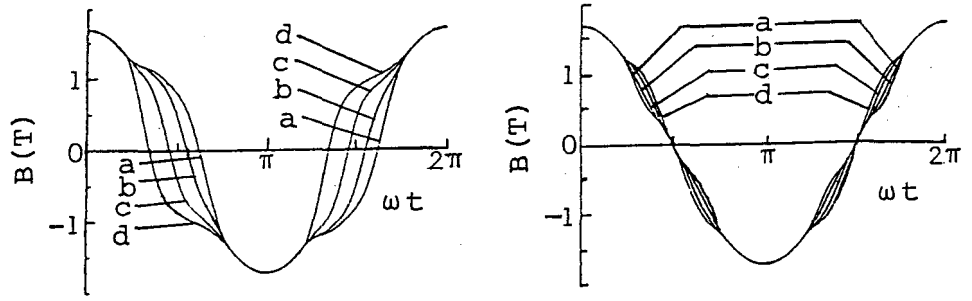

(a) with hysteresis (b) without hysteresis

Fig.30 Waveforms of localized flux densities (M-4,0.3mm,Bleg=1.7T).

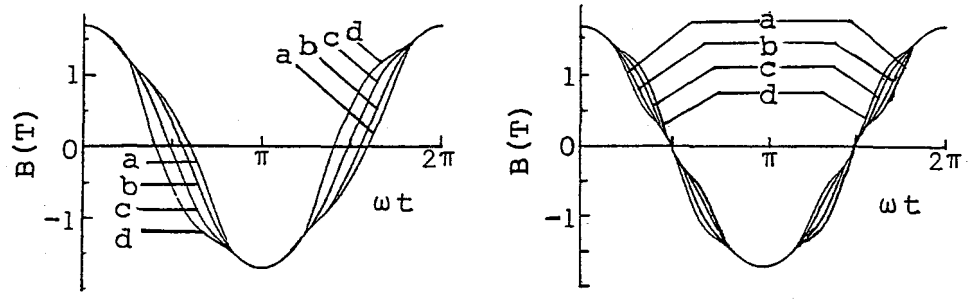

(a) with hysteresis (b) without hysteresis

Fig.31 Waveforms of localized flux densities (M-0H,0.3mm,Bleg=1.7T).

6. CONTROL OF FLUX DISTRIBUTIONS[19]

6.1 Outline

Iron losses in electrical machinery are increased by the spatial inequality of the flux distribution, the distortion of flux waveform etc. If the waveform of flux density and its maximum value are controlled, a smaller core with higher efficiency can be designed.

Control of flux can be carried out by adjusting the reluctances of the magnetic circuits. The reluctances can be changed by modification of the shape of the core and the magnetization curve of the material used. These can also be changed by the variation of joint configuration and the magnetic anisotropy of silicon steel.

In conventional research, the manufacturers of silicon steels and those of transformers have independently investigated the optimum magnetic characteristics of the silicon steel and the optimum construction of the transformer core respectively by trial and error. Therefore, it was impossible to examine the optimum transformer core in the synthetic point of view. Recently, with the rapid development of numerical methods such as the finite element method, it has become possible to investigate the above-mentioned problems quantitatively. The transformer manufacturers have reached the stage to specify that steel manufacturers produce silicon steel with the most preferable magnetic characteristics for transformer cores from the point of view of the optimum design.

On the other hand, although the steel manufacturers should produce silicon steel having the magnetic characteristics desired by the transformer manufacturers, the history of the developments of silicon steels shows that they have been keen to develop highly-oriented and low loss silicon steel in the rolling direction and they had never considered the above-mentioned problems.

A method for designing cores in which the flux distribution and the flux waveform in each part are optimized has been developed[19].

6.2 Method of Controlling Flux Distributions

For simplicity, the method is explained by an example shown in Fig. 32 (a). Figure 32 (b) shows the electrical equivalent circuit for a quarter of a single-phase transformer core. $R\ell_1,---,R\ell_4$ and $Ry_1,---,Ry_4$ denote the reluctances of the limb and the yoke respectively. As $R\ell_1<R\ell_2<R\ell_3<R\ell_4$ and $Ry_1<Ry_2<Ry_3<Ry_4$ the relationship among fluxes ϕ_1 through ϕ_4 in Fig.32 (b) becomes $\phi_1>\phi_2>\phi_3>\phi_4$, and the waveforms of these fluxes are distorted. The uniform flux distribution can be obtained using adequate reluctances $Rg_1,---,Rg_4$ in the magnetic circuits. $Rg_1,---,Rg_4$ are easily realized by some materials whose reluctances differ from that of the iron core, for example, air gap shown in Fig. 32 (c). The values of the additional reluctances are numerically calculated by using the

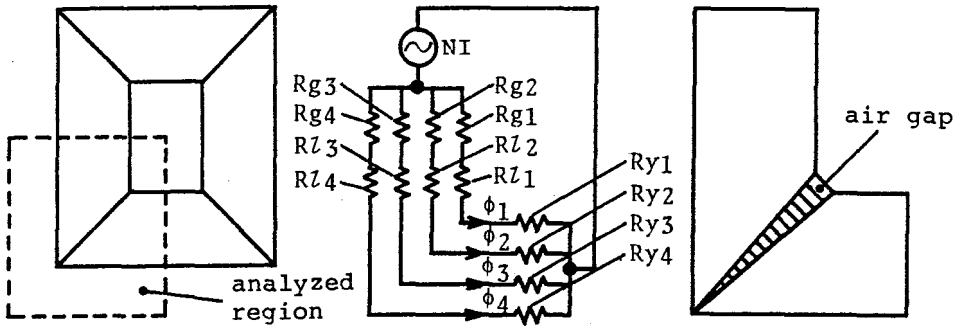

(a) single-phase transformer core (b) equivalent circuit (c) control of magnetic characteristics

Fig.32 Control of flux distribution.

"finite element method for the inverse problem" which was newly developed by us[20,29].

6.3 Examples of Control

Figure 33 shows an analyzed model which is 1/8 of a single-phase, two-limbed transformer core similar to that in Fig. 32 (a). The analyzed core is made of highly oriented silicon steel M-OH. Figure 34 (a) shows the waveforms of flux density at the joint. The waveform in each part is distorted, and the maximum value of the waveform B1 is larger than that of B6. This is caused by the differences between the magnetic path lengths and by magnetic saturation. Figure 34 (b) denotes the waveforms corresponding to Fig. 32 (c) which is controlled by inserting an air gap at the joint so that the maximum value of each waveform can be the same. Figure 34 (c) shows the other controlled waveforms. In this case, the air gap is inserted so that the waveform in every part can be approximately the same. The waveforms obtained are nearly sinusoidal.

7. ESTIMATION OF IRON LOSSES

A reliable method for estimating iron losses should be established in order to analyze the iron loss distribution from the flux distribution obtained numerically.

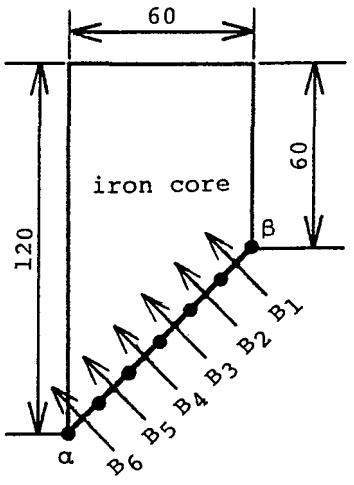

Fig.33 Analyzed model.

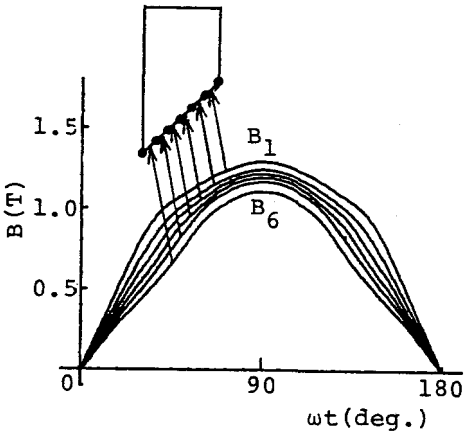

(a) without special control

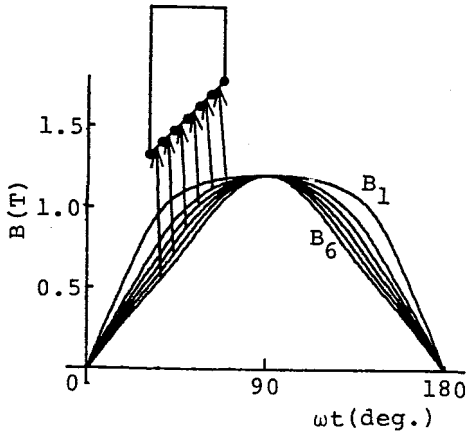

(b) with special control so that the maximum values can be the same

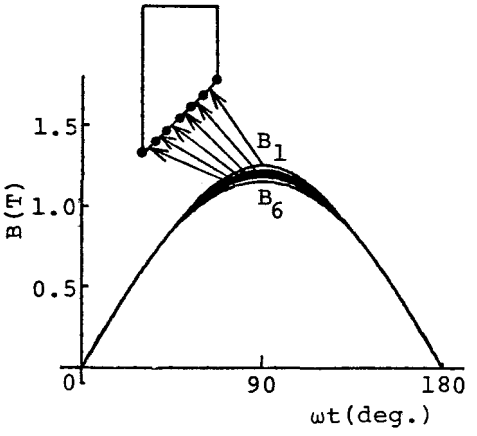

(c) with special control so that the distortions can be reduced

Fig.34 Waveforms of flux densities at the joint (M-0H,0.3mm,Bleg=1.7T).

7.1 Iron Losses due to Distorted Fluxes

In highly-oriented cores, the fluxes are considerably distorted due to the nonuniform flux distribution and circulating flux as mentioned in Section 3. Also, a high level of harmonic flux exists in the single-phase, four-limbed core and in the three-phase, five-limbed core due to magnetic saturation and the different path

lengths of the magnetic circuits.

Let us assume that the instantaneous flux density b is given by,

$$b = B_1 \sin \omega t + \Sigma B_n \sin n(\omega t + \theta_n) \quad \text{---------- (7)}$$

where B_1 and B_n are the amplitudes of the fundamental and the n-th harmonic component respectively, and θ_n is the phase angle of the n-th harmonic component. Σ represents the summation for all components.

The iron loss due to the distorted flux can be estimated by the following equations[21].

$$W = W_h + W_e \quad \text{---------- (8)}$$

$$W_h = w_h(B_m) + 2\sum_{i=1}^{m} w_h(B_{ki}) \quad \text{---------- (9)}$$

$$W_e = w_e(B_e) \quad \text{---------- (10)}$$

Where

W_h: hysteresis loss (W/kg)

W_e: eddy current loss (W/kg)

$w_h(B_m)$: function of hysteresis loss

$w_e(B_e)$: function of eddy current loss

B_e is the maximum flux density of the sinusoidal wave which has the same effective voltage as that corresponding to the distorted flux. Hence, B_e is defined by the following equation.

$$B_e = \sqrt{\Sigma (nB_n)^2} \quad \text{---------- (11)}$$

B_{ki} is the amplitude of the minor loop and m is the number of the groups of minor loops. Σ represents the summation of losses caused by the minor loops which appear in a half cycle successively. The functions w_h and w_e may be determined by the method for separating the hysteresis loss and the eddy current loss developed by us[21]. When the distorted flux contains large minor loops, the above-mentioned equations cannot be used[22].

The values of B_m, B_e and B_{ki} can be easily obtained from the numerical calculation.

When the flux flows in the rolling direction, the accuracy of Eq.(8) is within ±5% in the region of the flux density in practical use. When the flux does not flow in the rolling direction, the iron losses are usually estimated by the following equation[23].

$$W = W_R + W_T \quad \text{---------- (12)}$$

Where W_R and W_T denote the iron losses in the rolling and the transverse directions respectively. These are calculated from Eq. (8) by using the loss curves in the rolling and the transverse directions respectively. In this case, the flux densities B_m and B_e in Eqs. (9), (10) and (11) are those in the rolling and the transverse directions respectively. Equation(12) should be much more examined in order to establish the estimation method of iron losses in all directions.

7.2 Iron Losses due to Rotating Fluxes

Rotating fluxes exist in the T-joints of three-phase transformer cores due to three-phase magnetomotive forces. The locus of the rotating flux density vector becomes a flat ellipse due to the anisotropy of the silicon steel. The direction of the major axis of the ellipse does not always coincide with the rolling direction. When the flux density is high, the ellipse is distorted. This rotating flux causes a large addition to the total iron loss. Therefore, the establishment of a method for estimating the iron loss due to distorted rotating flux is desired.

The iron loss due to rotating flux without any harmonic component can be estimated from the lengths of the major and minor axes, and the angle between the direction of the major axis and the rolling direction[24]. When the rotating flux is distorted, the estimation of the iron loss is extremely difficult because the amplitude and the phase of the harmonic flux affect the iron loss.

It is very important to discuss the problems of iron losses. However, the present status of estimation techniques is not sufficient to discuss the problem of the building factor.

8. CONCLUSIONS

New knowledge obtained theoretically by numerical analysis can be summarized as follows:

(a) Although the total flux is sinusoidal, the localized flux is distorted due to the magnetic non-linearity and differences among magnetic path lengths.

(b) The building factor of the core made of highly-oriented silicon steel is larger than that of the conventional core.

(c) If the percentage of the area of the T-joints in a three-phase

transformer core is large, the building factor is increased.

(d) The transverse flux in the interlaminar gap concentrates near the joints at the instant when the flux density is the practical one.

(e) When the overlap length is increased, the eddy current losses at joints are increased and finally reach saturation.

(f) When the number of laminations per stagger layer is increased, the eddy current loss is rapidly increased and it is very much influenced by the air gap length in the joint.

(g) The iron losses are considerably increased by a small irregularity of the arrangement of sheets at the joint.

(h) The hysteresis characteristics should be taken into account in order to analyze accurately the waveform of flux.

(i) It is clarified that examinations of the optimum construction of core and the most desirable magnetic characteristics of core material are possible by using the finite element method.

Recent developments of laboratory automation system will enable us to examine easily the accuracy of numerical analysis.

Owing to the advent of the cheap personal computers with large memory, even the designer belonging to a small factory can analyze static non-linear magnetic fields in his office. Therefore, the optimum design method using numerical analysis will be widely used in daily design procedures.

If the estimation method of iron losses and the optimum design method can be established, the most suitable materials for transformer core and smaller cores with higher efficiency might be developed. Three-dimensional analysis of magnetic fields will also be introduced at reasonable cost in the near future. Then, a dramatic development might be expected in our field again. I hope for the co-investigation of transformer manufacturers and steel manufacturers in order to develop the most suitable magnetic material for transformer cores.

REFERENCES

(1) Y. Ishihara, T. Nakata and K. Yasuhara: "Effects of Magnetizing Characteristics of Silicon Steel on the Properties of Transformer Cores", Papers of Technical Meeting on Magnetics, MAG-81-28, IEE Japan (1981).

(2) M. Okabe, M. Okada and H. Tsuchiya: "Effects of Magnetic

Characteristics of Materials on the Iron Loss in the Three Phase Transformer Core", IEEE Transactions on Magnetics, Vol. MAG-19, No. 5 (1983) (to be published).

(3) T. Nakata and N. Takahashi: "The Finite Element Method in Electrical Engineering", Tokyo, Morikita Publishing Co. Ltd. (1982) (book).

(4) T. Nakata, Y. Ishihara and N. Takahashi: "Numerical Solution of Flux Distributions in Transformer Cores", International Symposium on Electrodynamics, Forces and Losses in Transformers, C2 (1979), pp. 243-254.

(5) T. Nakata: "Analysis of Flux Distribution of Three-Phase, Three-Limbed Transformer Cores", Electrical Engineering in Japan, Vol. 95, No. 3 (1975), pp. 43-50.

(6) T. Nakata, Y. Ishihara, K. Yamada and A. Sasano: "Non-Linear Analysis of Rotating Flux in the T-Joint of a Three-Phase, Three-Limbed Transformer Core", European Physical Society Conference, Proceedings of Soft Magnetic Materials 2, 4-5 (1975), pp. 57-62.

(7) Y. Ishihara, T. Nakata and S. Matsumura: "Studies on Various Factors of Affecting Magnetic Characteristics of Transformer Cores by Using Finite Element Method", Papers of Technical Meeting on Magnetics, MAG-80-45,IEE Japan (1980).

(8) T. Nakata, Y. Kawase and M. Kawata: "Approximate Solution of Three-Dimensional Magnetic Field at Joints of Transformer Cores", Papers of Combined Technical Meeting on Rotating Machines and Static Apparatus, RM-83-92, SA-83-43, IEE Japan (1983).

(9) T. Nakata et al.: "Interdisciplinary Finite Element Analysis", Cornell University (1981) (book).

(10) Y. Ishihara, T. Nakata and T. Akou: "Analysis on Magnetic Characteristics of Three-Phase, Five-Legged Transformer Core Using Finite Element Method", Papers of Technical Meeting on Magnetic Materials, MAG-78-49, IEE Japan (1978).

(11) T. Nakata, Y. Kawase, M. Matsubara and S. Ito: "Analysis of Magnetic Characteristics of Electromagnets with Shading Coil by Using the Finite Element Method", Papers of Combined Technical Meeting on Rotating Machines and Static Apparatus, RM-82-37, SA-82-1, IEE Japan (1982).

(12) T. Nakata and Y. Kawase: "Finite Element Analysis of theMagnetic Characteristics in Straight Overlap Joints of Laminated Cores", Transactions of IEE Japan, Vol. 103-B, No. 5 (1983), pp. 357-364.

(13) T. Nakata and Y. Kawase: "Analysis of the Magnetic Characteristics in the Straight Overlap Joint of Laminated Cores", Electrical Engineering in Japan, Vol. 102, No. 1 (1982), pp. 78-87.

(14) T. Nakata, N. Takahashi and Y. Kawase: "Flux and Loss Distribution in the Overlap Joints of Laminated Cores", Journal of Magnetism and Magnetic Materials, Vol. 26, Nos. 1-3 (1982), pp. 343-344.

(15) T. Nakata, N. Takahashi and Y. Kawase: "Magnetic Performance of Step-Lap Joints in Distribution Transformer Cores", IEEE Transactions on Magnetics, Vol. MAG-18, No. 6 (1982), pp. 1055-1057.

(16) T. Nakata and Y. Kawase: "Numerical Analysis of Magnetic Characteristics of Transformer Cores with Step-Lap Joint", Transactions of IEE Japan, Vol. 103-B, No. 3 (1983), pp. 17-24.

(17) T. Nakata, Y. Kawase, K. Matsubara and T. Matsubara: "Non-Linear Field Analysis and Magnetic Losses in Silicon Steel Sheets, Taking into Account the Effects of Hysteresis and Eddy Current", Papers of Technical Meeting on Magnetics, MAG-80-58 (1980).

(18) T. Nakata, Y. Kawase and T. Tsuboi: "Analysis of Transformer Cores Taking into Account Hysteresis Characteristics", Outline Collections of Scientific Lectures, Magnetics Society of Japan (1983) (to be published).

(19) T. Nakata, N. Takahashi, Y. Kawase and K. Fujiwara: "Control of Flux Distributions in Transformer Cores", Journal of Magnetism and Magnetic Materials, Vol. 28, Nos. 1-3 (1984) (to be published).

(20) T. Nakata and N. Takahashi: "Direct Finite Element Analysis of Flux and Current Distributions under Specified Conditions", IEEE Transactions on Magnetics, Vol. MAG-18, No. 2 (1982), pp. 325-330.

(21) T. Nakata, Y. Ishihara and M. Nakano: "Iron Losses of Silicon Steel Core Produced by Distorted Flux", Electrical Engineering in Japan, Vol. 90, No.1 (1970), pp. 10-20.

(22) T. Nakata, Y. Ishihara and M. Nakano: "Experimental Studies of Various Factors Affecting Minor Loop Hysteresis Loss", Memoirs of the School of Engineering, Okayama University, Vol. 8, No.1 (1973), pp. 1-14.

(23) Y. Ishihara, T. Nakata and T. Akou: "Analysis on Magnetic Characteristics of Three-Phase Shell-Type Three-Limbed

Transformer Core Using Finite Element Method", Papers of Technical Meeting on Magnetic Materials, MGA-78-1, IEE Japan (1978).

(24) Y. Ishihara and N. Takahashi: "Iron Losses of Silicon Steel due to Rotating Fluxes", Memoirs of the School of Engineering, Okayama University, Vol 14, No.1 (1979), pp. 15-28.

(25) M. Enokizono and T. Yano: "Estimation of Iron Loss in the Wound-Core Type Transformer by the Finite Element Method with Special Element", Papers of Technical Meeting on Magnetics, MAG-83-64, IEE Japan (1983).

(26) T. Nakata, Y. Ishihara and N. Takahashi: "Analysis on Magnetic Characteristics of Single-Phase, Four-Limbed Transformer Cores", European Physical Society Conference, Proceedings of Soft Magnetic Materials 3, 11-2 (1977), pp. 351-358.

(27) T. Nakata, N. Takahashi, Y. Kawase, K. Misawa, M. Kuwata, Y. Matsubara and N. Komma: "Magnetic Field Analysis by Finite Element Method", Nisshin Technical Report, Vol. 26, No. 4 (1981), pp. 94-105.

(28) T. Nakata, Y. Kawase and H. Funakoshi: "Analysis of Magnetic Field in Leakage Transformer by Using the Finite Element Method", Outline Collections of Scientific Lectures, Magnetic Society of Japan, 15aC-3 (1982).

(29) T. Nakata, N. Takahashi, Y. Kawase and K. Fujiwara: "Determination of Sizes of Electrical Machinery by Using Gap Elements", Papers of Combined Technical Meeting on Rotating Machinery and Static Apparatus, RM-83-45, SA-83-35, IEE Japan (1983).

(30) T. Nakata, Y. Ishihara and N. Takahashi: "Finite Element Analysis of Magnetic Fields by Using Gap Element", Proceedings of Compumag Conference, 5-7 (1978).

(31) T.Nakata, Y. Ishihara, N. Takahashi and Y. Kawase: "New Efficient Techniques for Calculating Magnetic Fields Taking into Account Hysteresis Characteristics and Eddy Currents", Papers of Technical Meeting on Information Processing, IP-80-9, IEE Japan (1980).